ADVANCES IN ATMOSPHERIC SCIENCES, VOL. 36, MARCH 2019, 326–338

• **Original Paper** •

Evaluation of Summer Monsoon Clouds over the Tibetan Plateau Simulated in the ACCESS Model Using Satellite Products

Liang HU[1,4], Zhian SUN[2], Difei DENG[*3,4], and Greg ROFF[2]

[1]*State Key Laboratory of Severe Weather, Chinese Academy of Meteorological Sciences, Beijing* 100081*, China*

[2]*Science to Services, Australian Bureau of Meteorology, Melbourne, Victoria* 3001*, Australia*

[3]*Institute of Atmospheric Physics, Chinese Academy of Sciences, Beijing* 100029*, China*

[4]*School of Physical, Environmental and Mathematical Sciences, The University of New South Wales, Canberra ATC* 2600*, Australia*

(Received 7 April 2018; revised 22 September 2018; accepted 19 October 2018)

ABSTRACT

Cloud distribution characteristics over the Tibetan Plateau in the summer monsoon period simulated by the Australian Community Climate and Earth System Simulator (ACCESS) model are evaluated using COSP [the CFMIP (Cloud Feedback Model Intercomparison Project) Observation Simulator Package]. The results show that the ACCESS model simulates less cumulus cloud at atmospheric middle levels when compared with observations from CALIPSO and CloudSat, but more ice cloud at high levels and drizzle drops at low levels. The model also has seasonal biases after the onset of the summer monsoon in May. While observations show that the prevalent high cloud at 9–10 km in spring shifts downward to 7–9 km, the modeled maximum cloud fractions move upward to 12–15 km. The reason for this model deficiency is investigated by comparing model dynamical and thermodynamical fields with those of ERA-Interim. It is found that the lifting effect of the Tibetan Plateau in the ACCESS model is stronger than in ERA-Interim, which means that the vertical velocity in the ACCESS model is stronger and more water vapor is transported to the upper levels of the atmosphere, resulting in more high-level ice clouds and less middle-level cumulus cloud over the Tibetan Plateau. The modeled radiation fields and precipitation are also evaluated against the relevant satellite observations.

Key words: Tibetan Plateau, cloud fraction, ACCESS model, COSP

Citation: Hu, L., Z. Sun, D. Deng, and G. Roff, 2019: Evaluation of summer monsoon clouds over the Tibetan Plateau simulated in the ACCESS model using satellite products. *Adv. Atmos. Sci.*, **36**(3), 326–338, https://doi.org/10.1007/s00376-018-7301-9.

1. Introduction

The dynamic and thermodynamic impacts of the Tibetan Plateau (TP) on atmospheric circulation have been investigated by many scientists (Maussion et al., 2011; Luo et al., 2011; Duan et al., 2013; Wang et al., 2015; Wu et al., 2015). In these studies, the important role of the cloud systems over the TP on weather and climate around the TP has been extensively investigated in the past several decades, but the particular characteristics of these cloud systems are not well understood, due to the complex topography and lack of sufficient observations over the TP. Remote sensing data from satellites have greatly enriched our knowledge of clouds over the TP since the 1970s (Yan et al., 2016). Recent satellite-retrieved products from CloudSat and CALIPSO (Marchand et al., 2008) have provided information on the cloud microphysical properties and their vertical distributions, which can be used to validate model cloud properties (Bodas-Salcedo et al., 2008; Stein et al., 2015). Through analysis of these satellite data, Luo et al. (2011) found that the deep convection on the TP is shallower, less frequent, and embedded in smaller-size convection systems than that along the southern slope of the TP and the regions of the southern Asia summer monsoon. They also found that the cloud-top height over the TP is lower than that of the southern slope region of the TP. A similar study was also conducted by Yan et al. (2016). They found that the frequency of a single-layer cloud over the TP was higher than those over the southern slope of the TP and the tropical ocean. The thickness of the single-layer cloud over the TP was comparable with that over the tropical ocean, while that over the southern slope region was much thicker, due to abundant moisture supply and strong upward motion (Yan et al., 2016).

There have been many numerical modelling studies that have examined the effects of the TP on the Asian summer monsoon (e.g., Wu and Zhang, 1998; Liu et al., 2007; IPCC, 2007; Annamalai et al., 2007). Duan et al. (2013)

* Corresponding author: Difei DENG
Email: ddfttkl@gmail.com

analyzed the TP summer monsoon using 15 CGCMs and eight AGCMs from CMIP5. They showed that GCMs are able to successfully simulate the climatological-mean monsoon over the TP, but large biases exist in the summer precipitation. Increasing the model spatial resolution and incorporating the indirect effects of sulfate aerosol helped to improve the model performance. Using ECHAM5 coupled with the ocean model developed by Max Planck Institute for Meteorology and atmosphere-only ECHAM5 models, Fallah et al. (2016) showed that the large-scale patterns of the Asian summer monsoon change significantly after removing the TP. Maussion et al. (2011) used the WRF model with different resolutions to evaluate precipitation over the TP and found that the simulated precipitation with higher spatial resolution was generally better than with lower resolution, but the precipitation bias due to the effects of the orography remains unsolved.

It can be seen from the literature that many studies have focused on the dynamic and thermodynamic effects of the TP on large-scale circulations, particularly those of the Asian monsoon. However, research activities comparing in detail the modeled and observed cloud properties over the TP seem to be insufficient. Such a study is important for improving the model physics and reducing the simulation biases in this region. For this reason, this study analyzes the cloud and radiative properties in the Australian Community Climate and Earth System Simulator (ACCESS) model and compares the simulation with the same properties derived from satellite observations. To ensure a consistent comparison between model output and satellite observation, the software of the Cloud Feedback Model Intercomparison Project Observation Simulator Package (COSP; Bodas-Salcedo et al., 2011) has been implemented in the ACCESS model (Franklin et al., 2013a). Thus, the modelled and satellite-retrieved cloud properties are determined in the same manner.

The paper is organized as follows: Section 2 introduces the data and model. Section 3 compares clouds over the TP between observations and simulations in boreal summer. Section 4 analyzes the dynamic and thermodynamic fields over the TP, as well as the surface energy budget and precipitation, to investigate the possible reasons for the differences between the model and observations. The last section discusses the key points of the study and draws conclusions.

2. Data and model

2.1. *Cloud data from CloudSat and CALIPSO*

Observational COSP datasets are used in this paper to validate the model-simulated cloud properties over the TP. In addition to the common cloud products retrieved from satellite observations, the CloudSat and CALIPSO products in COSP provide the vertical distributions of the cloud fractions and equivalent cloud microphysical properties. CloudSat provides multi-level cloud fractions and radar reflectivity, while CALIPSO produces multi-level lidar scattering ratio (SR) data. These datasets can be used to analyze the three-dimensional structures of clouds over the TP and validate the modeled results. The CALIPSO cloud fraction and SR are derived using the GCM-Oriented CALIPSO Cloud Product (GOCCP) (Chepfer et al., 2010), which diagnoses cloud properties from CALIPSO observations in the same way as in the model simulator. This ensures that discrepancies between the model and observations reveal biases in the model's cloudiness, rather than differences in the definition of clouds or diagnostics. The SR, which is proportional to the cloud optical depth, is defined as

$$\mathrm{SR}(z) = \frac{\mathrm{ATB}(z)}{\mathrm{ATB}_{\mathrm{mol}}(z)} ,$$

where ATB is the attenuation backscattered profile from the 532-nm CALIOP lidar level-1 dataset, $\mathrm{ATB}_{\mathrm{mol}}$ is the corresponding value in cloud-free conditions, representing the attenuated backscatter molecular signal profile, and z is the height of the ATB profiles. An atmospheric layer with $\mathrm{SR} > 5$ is classified as cloudy, while $0.01 < \mathrm{SR} < 1.2$ is clear, $1.2 < \mathrm{SR} < 5$ is unclassified, and $\mathrm{SR} < 0.01$ indicates the lidar signal is fully attenuated by a thick cloud above that layer. The monthly cloud fractions are determined at each vertical level by dividing the number of cloudy profiles identified during the month by the total number of SR profiles measured during that month.

2.2. *ERA-Interim data*

To evaluate the dynamic and thermodynamic fields in the ACCESS model, ERA-Interim (Dee et al., 2011) data are adopted. This dataset covers the period from January 1979 onwards and continues to be extended forward in near-real time. A large amount of observational data have been assimilated into the reanalysis, and these data are normally regarded as the best estimate of the state of the atmosphere. The temperature, moisture and wind fields for the same period as the CALIPSO/CloudSat observations are used to evaluate corresponding model variables. In addition, the cloud fraction and sensible and latent heat fluxes estimated by ERA-Interim are also used for model evaluation.

2.3. *Precipitation data*

For evaluating the model's precipitation fields, we collected three satellite-observed precipitation datasets. These precipitation data are: (1) Tropical Rainfall Measuring Mission (TRMM) (Huffman et al., 2010), designed to monitor tropical and subtropical precipitation and the associated energy balance—a joint space mission between NASA and the Japan Aerospace Exploration Agency. The mission delivered 17 years of precipitation data at a spatial resolution of 0.25°, covering 50°N to 50°S for 1998–2015 (product 3B42; Kummerow et al., 2001); (2) Global Precipitation Climatology Project (GPCP) (Adler et al., 2012), which comprises monthly satellite-gauge precipitation computed from microwave and infrared sounder data observed by the International Constellation of Precipitation-related Satellites; and (3) CPC Merged Analysis of Precipitation (CMAP) (Xie and Arkin, 1997), which is derived from a combination of gauge

data, satellite estimates, and NCEP–NCAR reanalysis, and comprises monthly mean data with a global coverage at a spatial resolution of 2.5° × 2.5°.

2.4. *Radiation data*

The Surface Radiation Budget (SRB) project is a NASA/GEWEX project for the retrieval of surface radiative fluxes from satellite observations (Zhang et al., 2015). This dataset provides shortwave and longwave radiation on a global grid of 1° × 1° at three-hourly intervals using the algorithms of Pinker and Laszlo (1992) and Fu et al. (1997). The data have a record length of 24 years from 1983 to 2007. These data are used in this work to evaluate the modeled radiation at the surface and the top of the atmosphere.

2.5. *ACCESS model*

The ACCESS model is used in this work to examine modelled cloud properties over the TP. A detailed description of the ACCESS model has been documented previously by Bi et al. (2013). Briefly, however, the ACCESS model is a coupled ocean and atmosphere climate modeling system developed at the Collaboration for Australian Weather and Climate Research. It uses the UK Met Office Unified Model (MetUM; Walters et al., 2017) as its atmospheric component, and in this study we conducted an atmosphere-only model run. ACCESS MetUM, version 10.1, was run for 30 years with: September 1988 initial conditions; a horizontal resolution of 1.25° latitude by 1.875° longitude; and 85 vertical levels. Prescribed sea-surface temperature and sea-ice data with seasonal variations were used as forcing from the ocean. The simulated results for January 2006 to December 2012 period, with three-hourly model outputs, were used to generate the satellite-equivalent cloud products. These model outputs were then used to compare with observed cloud properties over the TP.

The scheme to simulate subgrid variability in the computation of the radar reflectivity is SCOPS (the Subgrid Cloud Overlap Profile Sampler), developed for the ISCCP (International Satellite Cloud Climatology Project) simulator (Webb et al., 2001). The subgrid distribution of clouds is generated within a grid box by dividing the grid box into a number of vertical columns using a pseudorandom sampling process, fully consistent with the maximum, random and maximum/random cloud overlap assumptions. Maximum overlap is used for the convective cloud, and maximum/random is specified to the large-scale cloud. The convective and large-scale cloud water contents are distributed evenly in the subcolumns that are occupied by convective and large-scale cloud, respectively. Thus, the subgrid distribution in this case only accounts for cloud overlap assumptions, but not for the subgrid distribution of cloud water itself.

The subgrid sampling data are aggregated to produce a final product at the model grid box resolution. In this study, model outputs are analyzed from the CloudSat and CALIPSO simulators. The monthly mean cloud products are produced from daily means of three-hourly calculations, which are further averaged over the seven years to form a short-period climatology to compare with the satellite observations (CloudSat and CALIPSO).

3. Comparison of modelled and observed cloud properties over the TP in boreal summer

Figure 1 compares the total cloud fraction in boreal summer [June–July–August (JJA)] between CALIPSO observations and the ACCESS model simulation. Note that the total cloud fractions are determined using the maximum and random overlap assumption in both the model and satellite observation (Franklin et al., 2013b). CloudSat/CALIPSO observations (Fig. 1a) show that the largest cloud fraction occurs over the southern slope of the TP, with values decreasing northward and minimum values occurring over the northwestern TP. The ACCESS model captures the main distribution pattern of cloud fraction successfully, but produces a negative bias over the main, western and northeastern TP regions. As we know, most Tibetan convective systems occur over the

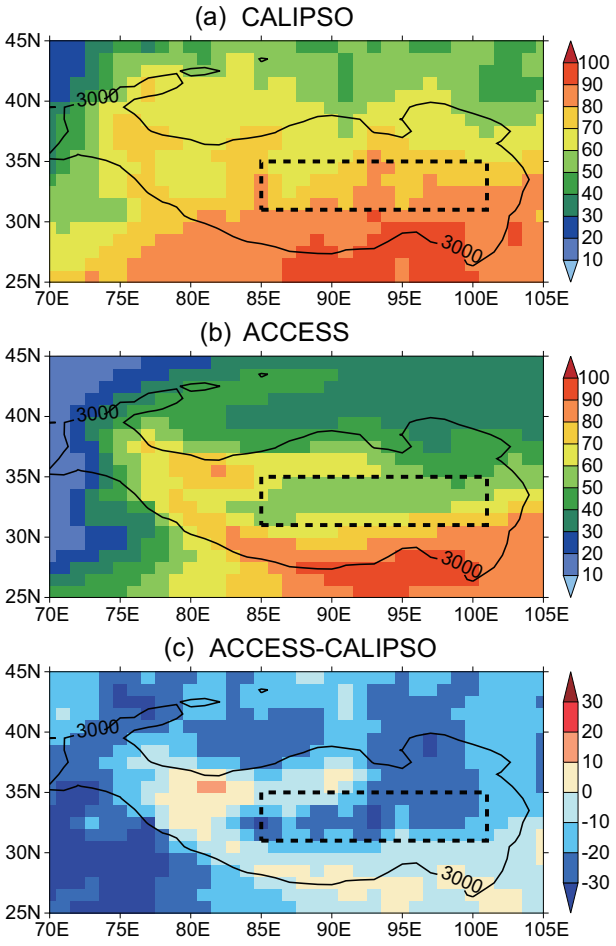

Fig. 1. Total cloud fraction over the TP in (a) CALIPSO and (b) ACCESS, and (c) the difference between them, in JJA. Units: %. The black contour represents the 3000 m topography. The dashed box (31°–35°N, 85°–101°E) shows the main region of the TP selected in this study.

central and eastern part of the TP (Gao et al., 1982; Hu et al., 2017), so the region (31°–35°N, 85°–101°E) was selected in this study to investigate the possible reasons for the cloud deficiency over the TP.

Unlike conventional passive sensor satellites, CloudSat/CALIPSO can provide the vertical distribution of cloud. The vertical cloud fraction difference between the model and observation is shown in Fig. 2, where Fig. 2a shows a longitude–height cross section and Fig. 2b a latitude–height cross section of the cloud fraction difference. It can be seen that the model produces more cloud over the TP at the heights of 11–16 km, especially over the south slope (> 25%). The result is opposite to the result over the West African monsoon and Indian monsoon regions, where high-level clouds in the model are much less than observed (Stein et al., 2015; Jayakumar et al., 2017). Compared to satellite observation, ACCESS generates less cloud at heights between 7 and 11 km, and this negative bias can be lower than −25%. The results from Figs. 1 and 2 indicate that the total cloud fraction over the main TP region is underestimated by the ACCESS model, and this underestimation is due to a failure to produce enough middle-level clouds in the model, despite producing more cloud at high levels.

CloudSat provides radar reflectivity determined via a reflecting particle size distribution scattering program (Pokharel and Vali, 2011), and can estimate the number and sizes of scattering particles. Figure 3 shows the CloudSat and ACCESS reflectivity–height histograms over the main TP region (the dashed box in Fig. 1). The observed reflectivity shows that cloud particles are constrained between 5 and 15 km in the vertical, while modeled values extend both above and below those levels, suggesting that more and deeper convection occurs in ACCESS. The observed reflectivity cuts off at −30 dBZ, whereas the modeled values extend to −40 dBZ, indicating that the model produces more small particles than in the satellite observations. The modeled highest frequency corresponds to a reflectivity of −5 to 10 dBZ and appears at ~ 5 km. Abel and Boutle (2012) identified that this problem is due to more drizzle-sized drops being produced by the model.

Figure 3a shows that the observed highest occurrence centers around 7 km in the radar reflectivity range of −15 to 0 dBZ, corresponding to the prevalent cumulus clouds over the TP (Gao et al., 1982), but the model does not capture this characteristic, instead producing higher values above and below the observed center (Fig. 3b). This means that ACCESS produces more small ice cloud particles than observed at levels above 11 km, and more drizzle-sized raindrops below 6 km. More small ice clouds at high levels demonstrates that deep convection in the model is too strong over the TP, while more drizzle-sized raindrops at low levels is similar to the situation elsewhere (Franklin et al., 2013b; Luo et al., 2016).

As the radar is insensitive to thin ice cloud, comparison of modeled lidar SRs with those from CALIPSO can further reveal the deficiency of the modeled cloud microphysical structure (Winker et al., 2010).

Figure 4 shows the SR distribution of CALIPSO lidar observations, wherein there are three large-frequency regions:

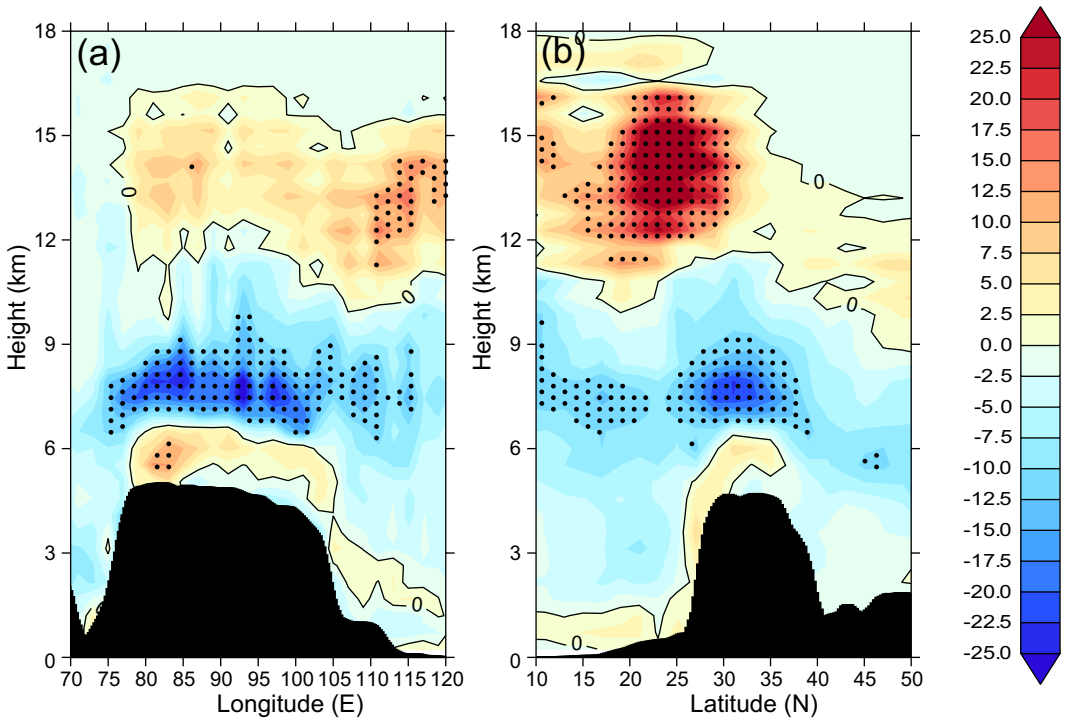

Fig. 2. Cloud fraction difference between ACCESS and CALIPSO in (a) longitude–height and (b) latitude–height cross sections over (31°–35°N, 85°–101°E) in JJA. Units: %. The dotted area shows differences larger than 10%.

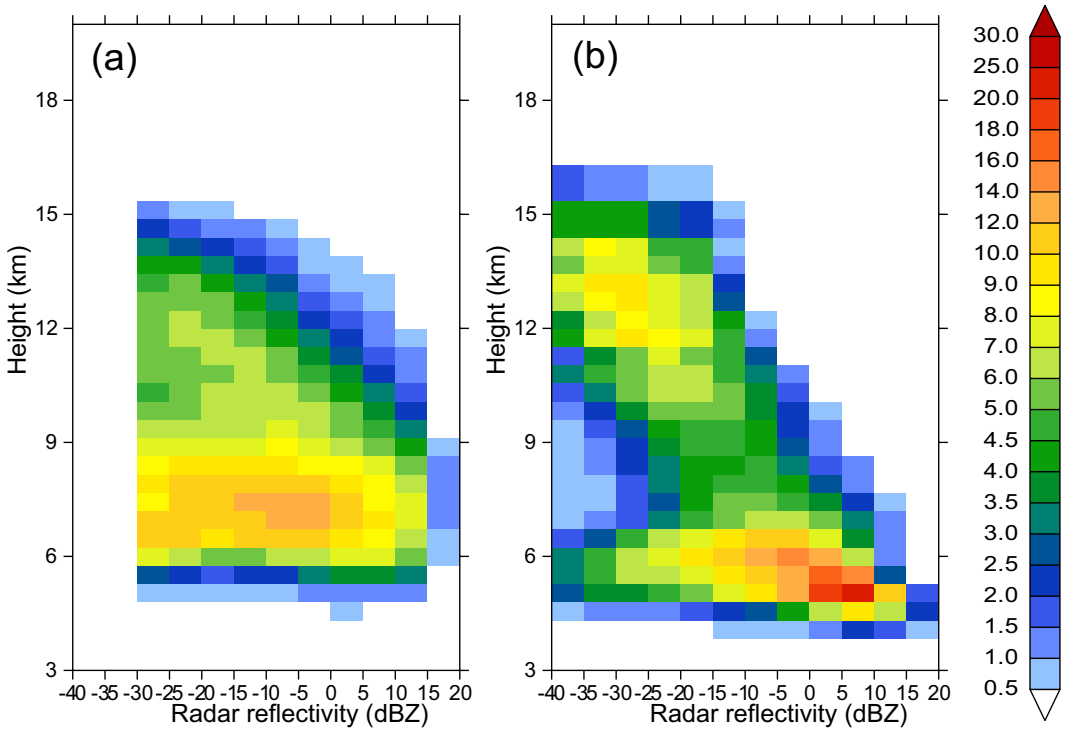

Fig. 3. Radar reflectivity–height histogram from (a) CloudSat observation and (b) the ACCESS radar simulator over the main TP in JJA. Units: 10^{-3}.

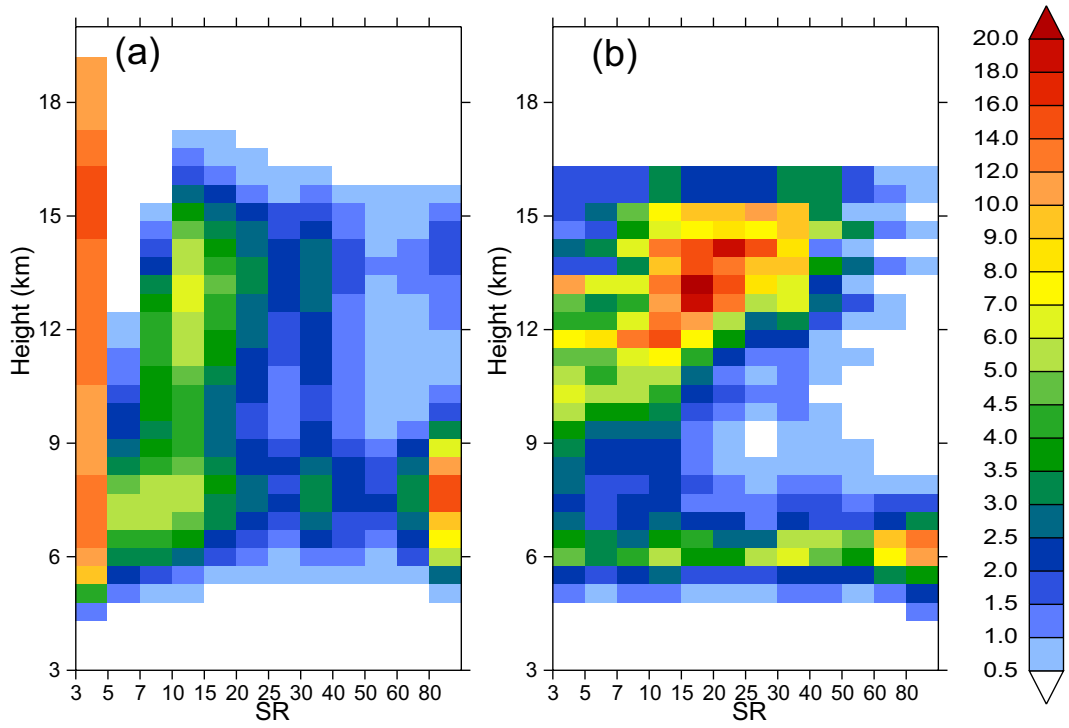

Fig. 4. Lidar SR–height histogram from (a) CALIPSO observation and (b) the ACCESS lidar simulator over the main TP in JJA. Units: 10^{-3}.

SR > 80 at 6–9 km; 7 < SR < 20 at 11–16 km; and 5 < SR < 20 at 6–9 km. The first region (SR > 80 at 6–9 km) has the largest frequency of occurrence. This region corresponds to typical cumulus clouds over the TP, but the modeled values are located at 5–7 km, about 2 km lower than observed. The second large SR region (7 < SR < 20 at 11–16 km) is produced by the deep convective cloud systems over the TP. The model captures the main feature of convective cloud between

11 and 16 km, but the frequency occurrences for SR between 7 and 40 are too high. This suggests that the model overestimates the ice cloud optical depth in the upper troposphere, indicating the model's deep convection over the TP in boreal summer is too strong. A third large region is observed, with SR between 5 and 20 at 6–9 km, in CALIPSO, but it is missed in ACCESS, reflecting the deficiency of low cloud water content in the model. Of note is that large frequencies for SR < 5 are observed at all levels by CALIPSO. Based on the GOCCP threshold definitions, these SR values indicate three cases: (1) atmospheric layers are cloud-free (0.01 < SR < 1.2); (2) the lidar signal is fully attenuated by thick cloud above that layer (SR < 0.01); and (3) layers can be unclassified because of the possible presence of subvisible cirrus clouds or aerosols (1.2 < SR < 5).

As we can see from Figs. 3 and 4, ACCESS simulates less Tibetan cumulus clouds at middle levels compared with CALIPSO and CloudSat observations, whereas it produces more small ice particles at high levels and more water content/raindrops at low levels.

We further examine the seasonal variation of clouds over the main TP, and Fig. 5 shows the month–height cross section of cloud fractions determined by CALIPSO, ACCESS, and ERA-Interim. Similar to the result of Yan et al. (2016), all datasets show a seasonal variation of the cloud fractions over the main TP: a single peak at 8–11 km from January to May, and two peaks at 6–9 km and 12–15 km from July to September. However, after the onset of the summer monsoon in May, the ACCESS 8–11 km maximum shifts to 12–15 km, while it shifts to 6–9 km in observations and reanalyses. Figure 5d shows the differences between simulated and observed cloud fractions, and one can see that there are large negative middle-level biases and positive biases aloft.

Cloud is one of the most difficult variables to simulate in numerical models, yet Fig. 5 shows that the seasonal variation of clouds over the main TP in ERA-Interim is very close to those of CALIPSO. As one of the best reanalysis datasets in the world, a large amount of observational data have been assimilated into ERA-Interim, and it has been widely used as the real state of the atmosphere for model evaluations. So, ERA-Interim is used as a reference in the following sections to diagnose the possible reasons that cause the biases of the cloud simulations in ACCESS in this study.

4. Investigation of the ACCESS model cloud bias

4.1. *Dynamic and thermodynamic fields*

To find possible reasons that may explain the ACCESS model errors, dynamic and thermodynamic fields generated by ACCESS and ERA-Interim are analyzed. Figure 6 shows TP month–pressure cross sections of relative humidity (RH), temperature, and vertical velocity from ERA-Interim and ACCESS.

ACCESS captures the main features of the seasonal variation of temperature; however, at levels above 250 hPa in JJA, the RH is larger and vertical velocity is stronger than in ERA-Interim. The strong vertical velocity in JJA brings more water vapor to upper levels, leading to the higher cloud fractions above 10 km (Fig. 5d). Note a large difference in RH between ACCESS and ERA-Interim occurs at the lower boundary, due to the boundary cutting through mountains for the ACCESS model, which is not applied in the ERA-Interim boundary condition.

Figures 7a and b show that the circulation and temperature around the TP are similar between ERA-Interim and ACCESS. The low-level southern air climbing over the TP

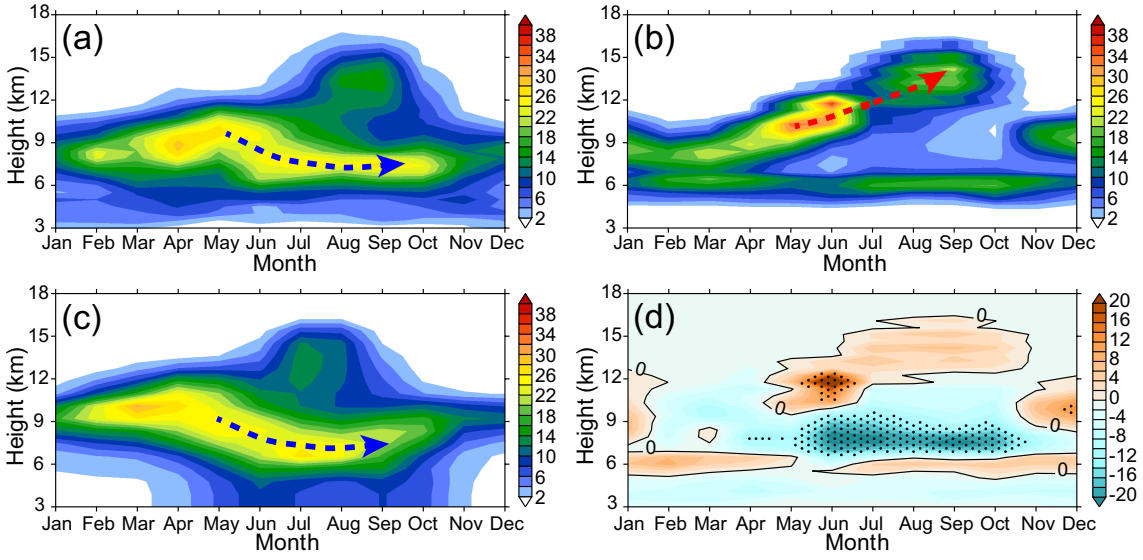

Fig. 5. Month–height cross section of cloud fraction over the main TP in (a) CALIPSO, (b) ACCESS, (c) ERA-Interim, and (d) the difference between ACCESS and CALIPSO. The black dotted area means the difference larger than 10%. The blue and red arrow represent the moving downward and upward of the cloud, respectively.

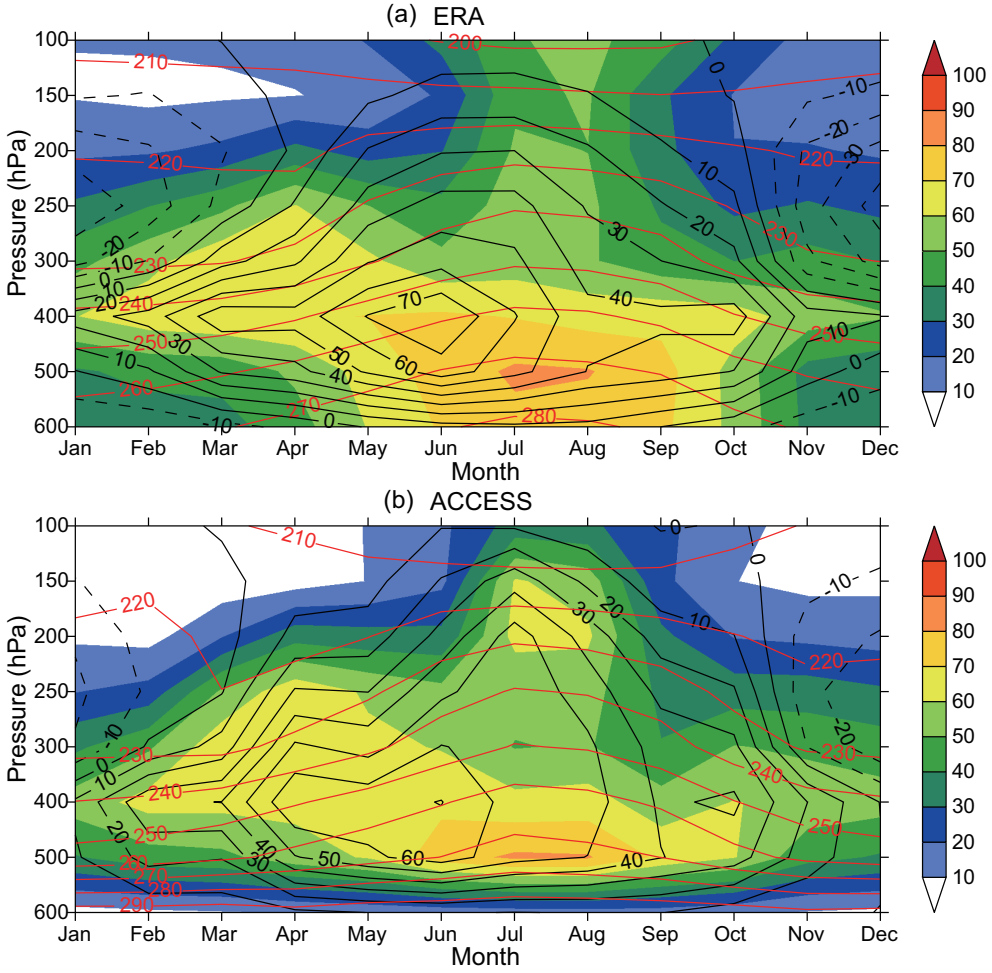

Fig. 6. Month–pressure cross section of RH (shaded, %), temperature (red contours, K), and vertical velocity (black contours) over the main TP in (a) ERA-Interim and (b) ACCESS. (the vertical velocity is multiplied by −1000 so that it has units of -10^{-3} Pa s^{-1}.)

southern slope, then turning back to tropical regions at high levels, is simulated successfully in ACCESS, but the vertical velocity at 850–200 hPa is overestimated over the TP southern slope, while it is underestimated over the Bay of Bengal (10°–20°N). Figure 7c shows the difference in wind and RH between ACCESS and ERA-Interim. Most of the vertical velocity over the TP is overestimated in ACCESS, especially over the southern slope, and the high-level RH is also overestimated over the TP.

Figures 6 and 7 suggest that the main reason for the ACCESS cloud simulation problem over the TP is that the lifting effect of the TP is stronger than in ERA-Interim, especially over its southern slope. The strong vertical velocity transports more water vapor to high levels, resulting in the higher frequency of ice cloud aloft (due to increased ice particle formation) and lower frequency of cumulus cloud at middle and low levels (due to reduced moisture content) over the TP.

4.2. *Surface energy budget*

To see if the surface heating on the TP is too strong in ACCESS, which may be partly responsible for its positive bias in convection and vertical velocity, the surface energy budget is analyzed using radiation data retrieved from the NASA/GEWEX SRB project.

Figure 8a shows the surface net shortwave radiation difference in JJA between the model and SRB observations. It can be seen that the net shortwave radiation over the main TP is overestimated by the ACCESS model, and the cloud shortwave radiative effect (CSRE) in this region is less than observed in terms of absolute values, leading to positive biases as shown in Fig. 8c. These results are consistent with the cloud distribution presented in the previous sections: the high clouds are overestimated, while the middle clouds are underestimated. Such cloud distributions allow more solar radiation to reach the surface and reduce the CSRE, leading to a positive bias in CSRE. More shortwave heating at the surface facilitates convection and makes the strong convection over the TP even stronger.

Figure 8b shows the biases of the outgoing longwave radiation (OLR) at the top of the atmosphere (TOA). Negative values mean underestimations of OLR in the model, and these are seen in the eastern, southeastern, and northwestern

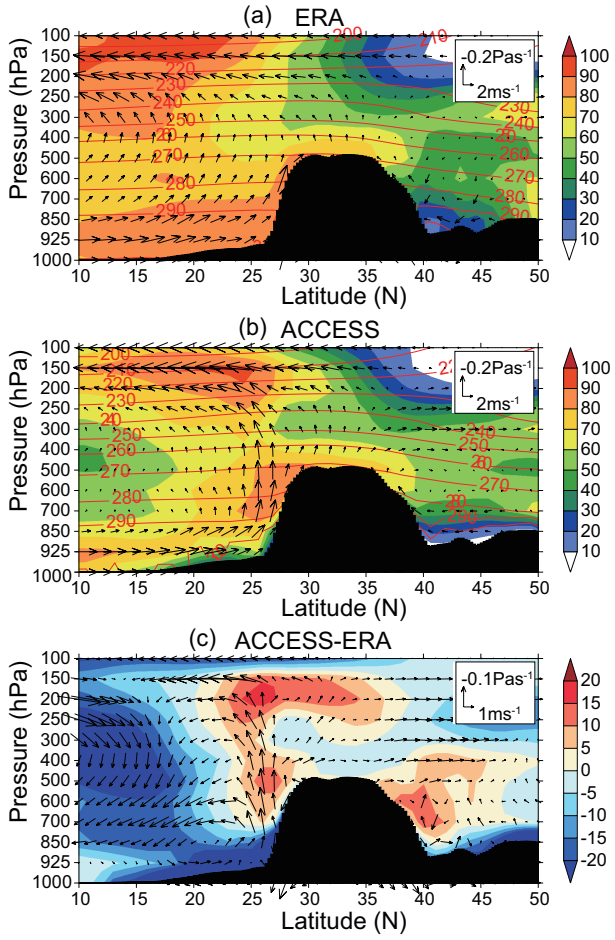

Fig. 7. Mean latitude–pressure cross sections of wind (vectors), RH (color shading, %), and temperature (contours, K) over 85°–101°E in (a) ERA-Interim, (b) ACCESS, and (c) their differences. The black shade represents the topography.

TP regions. The lower OLR means that the cloud-top heights are too high. The model overestimates the OLR in the western TP region. Figure 8d also shows a net upward longwave flux difference at the surface, which results in the main TP having very similar OLR differences at the TOA. The negative bias suggests that the modeled downward longwave flux is larger than observed, which may reflect the effect of high-level clouds and thus indicate a consistent cloud effect.

Figure 9 compares the sensible and latent heat flux between ACCESS and ERA-Interim. The model overestimates the sensible and latent heat fluxes over the main TP, and the overestimation of the latent flux spreads over the whole TP too. The seasonal variations of surface energy fluxes over the main TP are also calculated, as plotted in Fig. 10. Compared with ERA-Interim, the ACCESS model underestimates the sensible heat fluxes from January to March and overestimates them from May to June and August to December, while the model's latent heat fluxes are systematically overestimated throughout the year. These results indicate that the overestimation of sensible and latent heat fluxes by ACCESS may also be responsible for the strong summer convection over the main TP.

4.3. *Precipitation*

Strong convection must result in strong precipitation, and so evaluation of the model's precipitation can be used as evidence confirming the excessive convection. For this purpose, the precipitation is compared with three observed precipitation climatologies, based on retrievals from satellites, gauge observations, and reanalysis, respectively. These precipitation data, corresponding to the period of the model simulations (2006–12), are averaged for the summer mean and compared with the model's results.

Figure 11 shows that the distribution pattern of precipitation from the three observed climatologies are very similar, with large precipitation occurring on the southern slope of the TP and extending to the Bay of Bengal. Over the main part of the TP, the precipitation decreases from southeast to northwest. The distribution pattern produced by the ACCESS model shows high values in the south and low values in the north, which is quite different from the observation. The precipitation along the TP southern slope in ACCESS is much larger than observed, and overestimation is also apparent in the western and northwestern parts of the TP. These comparisons confirm that the ACCESS model overestimates the precipitation along the southern slope and main part of the TP. An overestimation of precipitation over the TP was also identified by Walters et al. (2017), using MetUM in both the GA4 and GA6 configurations, and the results presented here are consistent with their findings.

To analyze the precipitation more carefully, convective rain and large-scale rain need to be evaluated separately. Only TRMM data include convective and stratified components of precipitation, but these precipitation types over the TP region have been found to be unreliable (Fu and Liu, 2007), due to misidentified weak convective precipitation as large-scale precipitation, and therefore the results cannot be used for our purposes. Instead, the convective precipitation and large-scale precipitation from ERA-Interim are used in this study. Figures 12a and b compare the total precipitation between CMAP and ERA-Interim. It can be seen that the agreement between these two datasets is generally better than that between CMAP and the ACCESS model, albeit the results from ERA-Interim along the southern slope of the TP are less than those of CMAP. Figures 12c–f compare the convective and large-scale precipitation between the ACCESS model and ERA-Interim. It can be seen that ACCESS overestimates both large-scale and convective precipitation, but the overestimation of convective precipitation is much larger than that of the large-scale precipitation, especially along the southern slopes of the TP. This suggests that the total rainfall overestimation over the main TP in ACCESS is mainly due to the overestimation of convective precipitation.

5. Conclusions and discussion

Using the radar reflectivity and lidar SR dataset from CloudSat and CALIPSO, the horizontal and vertical distri-

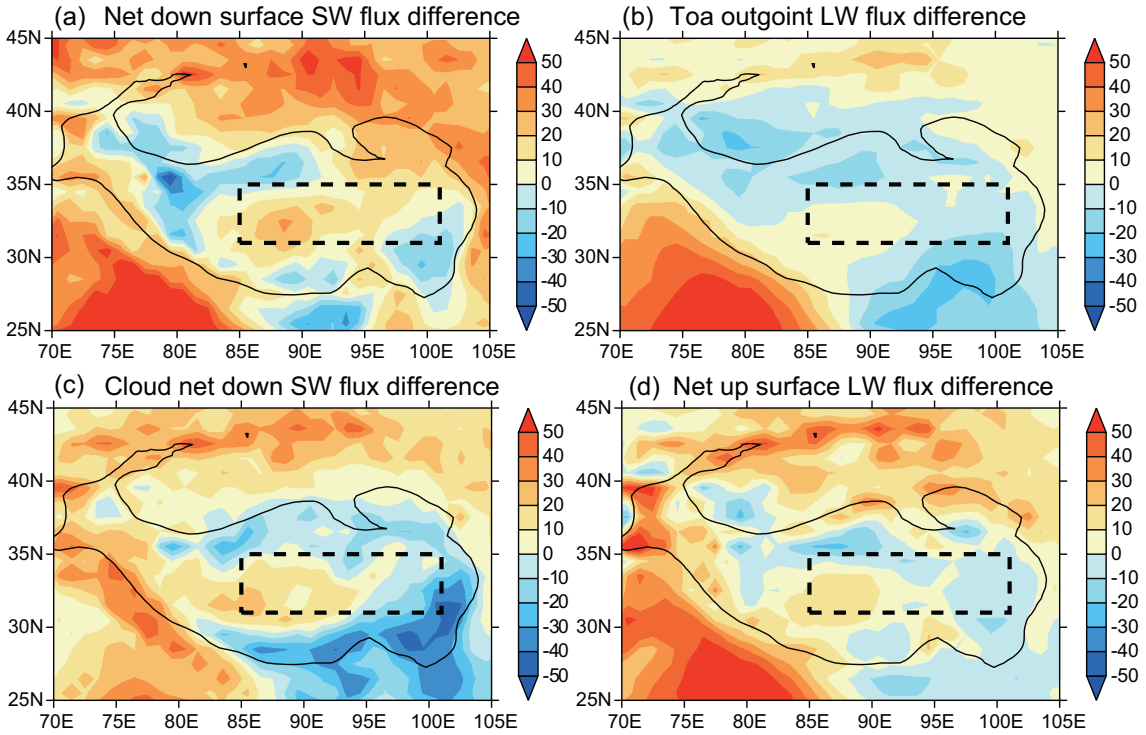

Fig. 8. Radiation difference between ACCESS and SRB for (a) net shortwave radiation at the surface, (b) OLR at the TOA, (c) the cloud shortwave radiative effect at the surface, and (d) net upward longwave radiation at the surface. Units: W m^{-2}. The black contour represents the 3000 m topography. The dashed box (31°–35°N, 85°–101°E) shows the main region of the TP selected in this study.

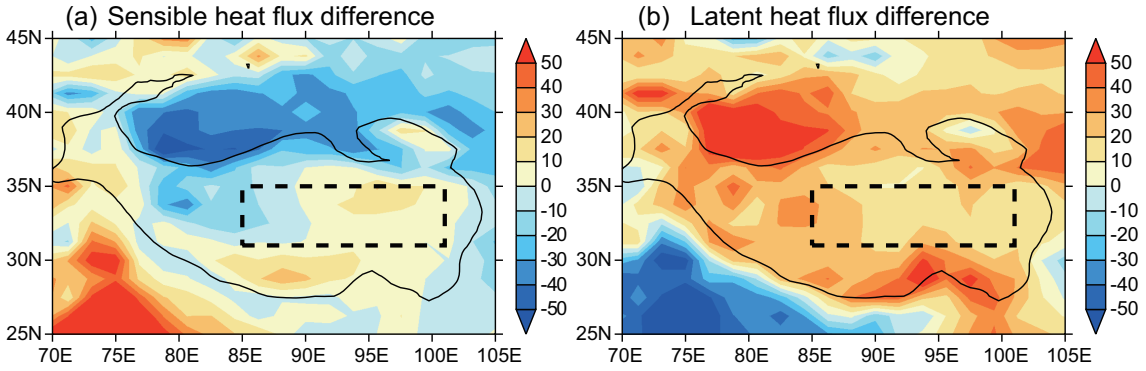

Fig. 9. (a) Difference in surface sensible heat flux between ACCESS and ERA-Interim. (b) As in (a) except for latent heat flux. Units: W m^{-2}. The black contour represents the 3000 m topography. The dashed box (31°–35°N, 85°–101°E) shows the main region of the TP selected in this study.

butions and seasonal variations of cloud properties over the TP in boreal summer simulated by the ACCESS model are evaluated in this paper.

The results show that the ACCESS model generates a lower frequency of cloud at 7–11 km over the TP, but a higher frequency of cloud at 11–16 km and below 7 km. These results indicate that ACCESS produces less cumulus clouds at middle levels, but more small ice particles at high levels and drizzle-sized drops at low levels.

The ACCESS model also produces biases in the seasonal variation of cloud fraction over the TP. With the onset of the summer monsoon in May, observations show that the maximum of cloud fractions occurring at 7–11 km in May descends to lower levels, at 6–9 km, over the main TP; whereas, it shifts upward to a higher level, at 10–15 km, in ACCESS simulations.

The dynamic and thermodynamic fields simulated by ACCESS are then compared with ERA-Interim data, showing that the vertical velocity over the TP is stronger than in ERA-Interim, especially on the TP's southern slope. The strong vertical velocity brings more water vapor to higher levels, resulting in more cloud at high levels and less cumulus cloud

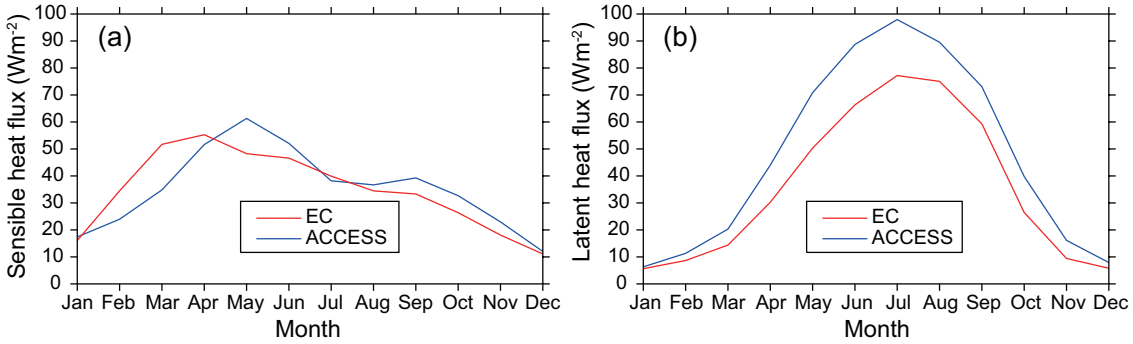

Fig. 10. Seasonal variations of surface (a) sensible heat flux and (b) latent heat flux over the main TP. Units: W m^{-2}.

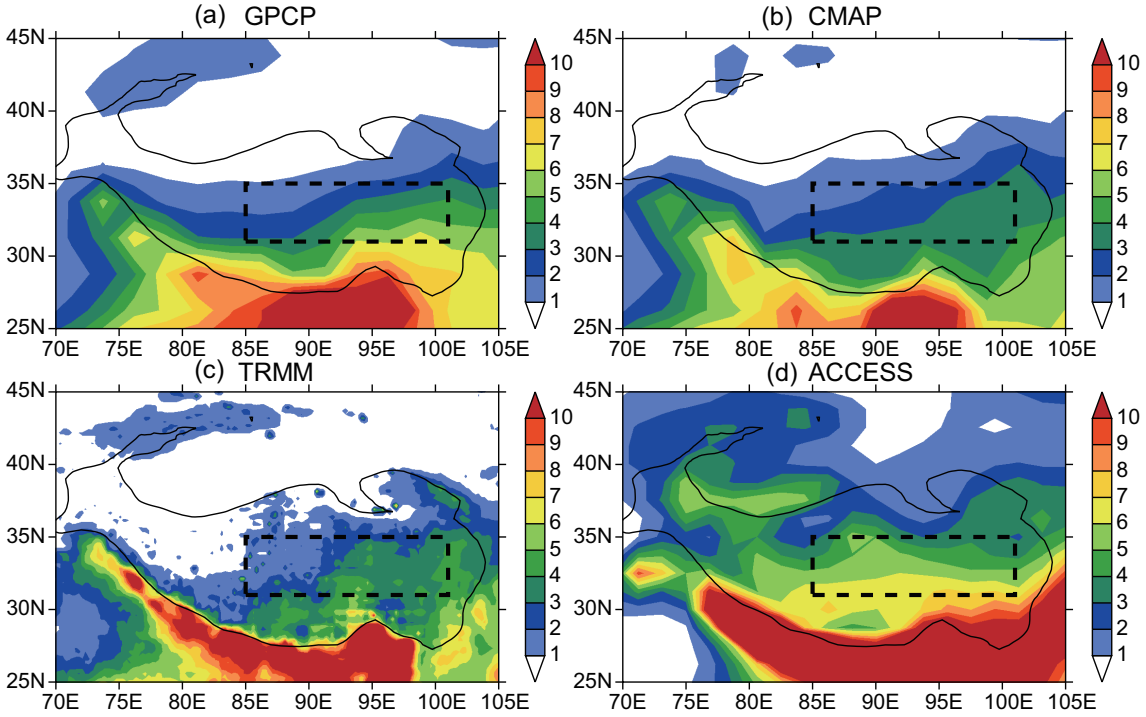

Fig. 11. Total precipitation (units: mm d^{-1}) in JJA determined by (a) GPCP, (b) CMAP, (c) TRMM, and (d) ACCESS. The black contour represents the 3000 m topography. The dashed box (31°–35°N, 85°–101°E) shows the main region of the TP selected in this study.

at middle levels. This suggests that the effects of topography and the boundary layer scheme in the ACCESS model may need to be adjusted in the TP region to reduce the lifting effect.

The surface radiation fields generated by ACCESS are evaluated against the same variables estimated from satellite measurements, while the sensible and latent heat fluxes are compared with ERA-Interim. The results show that the model overestimates the surface net solar radiation, sensible and latent heat fluxes, which may be a possible cause for the strong convection over the TP. The modeled precipitation is evaluated using three observational datasets estimated from satellites, revealing that the ACCESS model also overestimates precipitation along the southern slope and western and northwestern parts of the TP, especially for convective precipitation.

The model biases over the TP region explored in this study raise an unclear issue of positive feedback, i.e., whether the surface forcing produces convection that is too strong and leads to the incorrect vertical cloud structure, or it is the vertical cloud distribution that results in the incorrect surface radiative forcing. To answer this question, we intend to conduct some sensitivity studies to test the effects of some critical physical processes, such as convection, topography, and boundary conditions. Due to the complex topography in this area, especially along the south slope of the TP, the effect of model resolution may also have an important impact. These sensitivity studies will be conducted in the near future using the ACCESS city-scale model, with a relatively high spatial resolution.

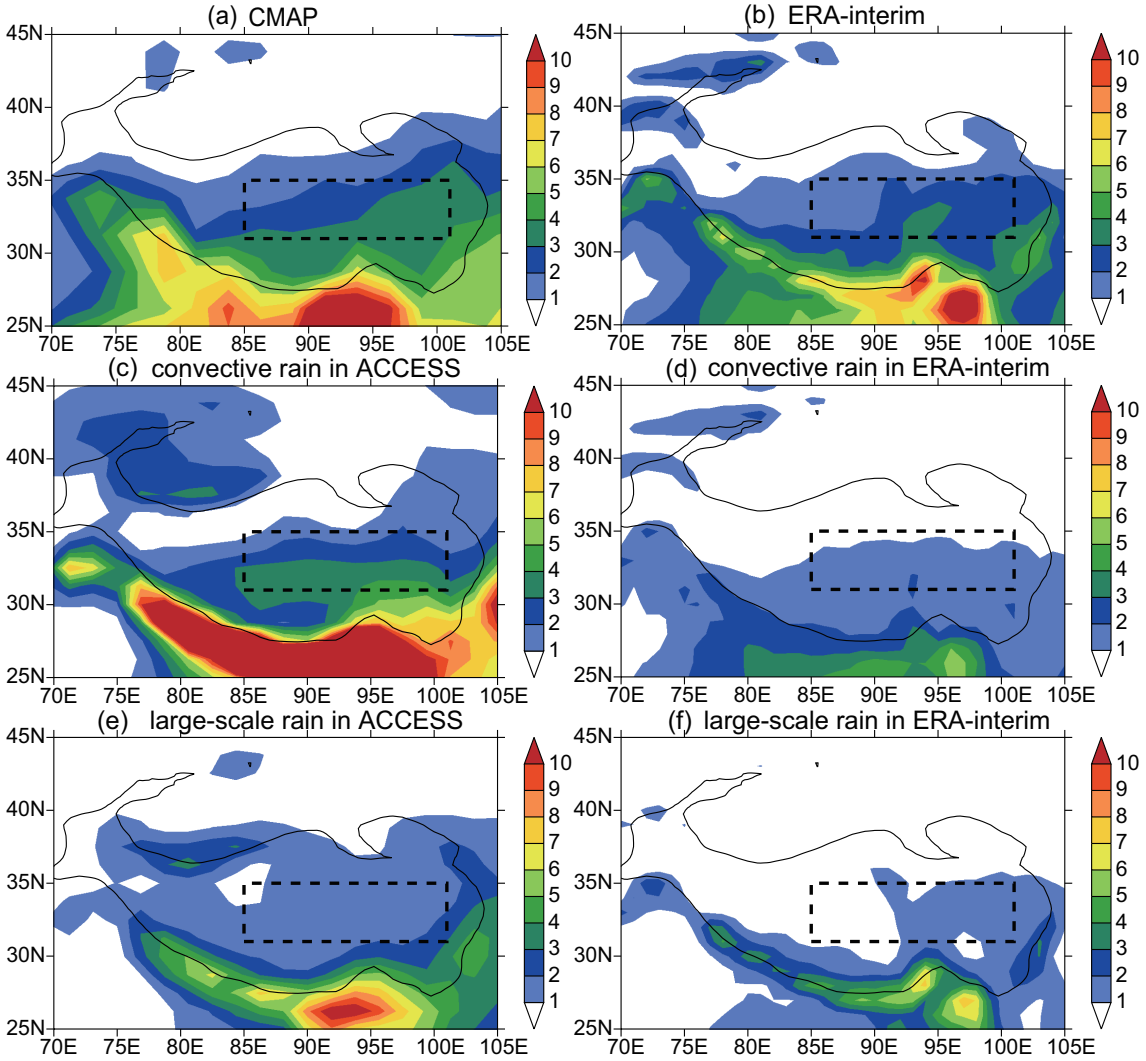

Fig. 12. Total precipitation in JJA determined by (a) CMAP and (b) ERA-Interim. (c, d) JJA convective precipitation in (c) ACCESS and (d) ERA-Interim. (e, f) JJA large-scale precipitation in (e) ACCESS and (f) ERA-Interim. Units: mm d^{-1}. The black contour represents the 3000 m topography. The dashed box (31°–35°N, 85°–101°E) shows the main region of the TP selected in this study.

Acknowledgements. Drs. Gary DIETACHMAYER, Hongyan ZHU, and Tony HIRST are thanked for internally reviewing this manuscript. This study was funded by the Third Scientific Experiment of the Tibetan Plateau (Grant No. GYHY201406001), the National Natural Science Foundation of China (Grant Nos. 41575045, 41205030, and 41175046), and the Basic Research Fund of the Chinese Academy of Meteorological Sciences (Grant No. 2017Z013). The authors would like to thank TRMM TSDIS for providing the TRMM 3B42 datasets (ftp://disc2.nascom.nasa.gov/ftp/data/s4pa/TRMM_L3/TRMM_3B42/). The CMAP precipitation data were provided by NOAA/OAR/ESRL PSD, Boulder, Colorado, USA, via their website at http://www.esrl.noaa.gov/psd/.

REFERENCES

Abel, S. J., and I. A. Boutle, 2012: An improved representation of the raindrop size distribution for single-moment microphysics schemes. *Quart. J. Roy. Meteor. Soc.*, **138**, 2151–2162, https://doi.org/10.1002/qj.1949.

Adler, R. F., G. J. Gu, and G. J. Huffman, 2012: Estimating climatological bias errors for the global precipitation climatology project (GPCP). *Journal of Applied Meteorology and Climatology*, **51**, 84–99, https://doi.org/10.1175/JAMC-D-11-052.1.

Annamalai, H., K. Hamilton, and K. R. Sperber, 2007: The South Asian summer monsoon and its relationship with ENSO in the IPCC AR4 simulations. *J. Climate*, **20**, 1071–1092, https://doi.org/10.1175/JCLI4035.1.

Bi, D. H., and Coauthors, 2013: The ACCESS coupled model: description, control climate and evaluation. *Australian Meteorological and Oceanographic Journal*, **63**, 41–64.

Bodas-Salcedo, A., and Coauthors, 2011: COSP: Satellite simulation software for model assessment. *Bull. Amer. Meteor. Soc.*, **92**, 1023–1043, https://doi.org/10.1175/2011BAMS2856.1.

Bodas-Salcedo, A., M. J. Webb, M. E. Brooks, M. A. Ringer, K. D. Williams, S. F. Milton, and D. R. Wilson, 2008: Evaluating cloud systems in the met office global forecast model using

simulated CloudSat radar reflectivities. *J. Geophys. Res.*, **113**, D00A13, https://doi.org/10.1029/2007JD009620.

Chepfer, H., S. Bony, D. Winker, G. Cesana, J. L. Dufresne, P. Minnis, C. J. Stubenrauch, and S. Zeng, 2010: The GCM-oriented CALIPSO cloud product (CALIPSO-GOCCP). *J. Geophys. Res.*, **115**, D00H16, https://doi.org/10.1029/2009JD012251.

Dee, D. P., and Coauthors, 2011: The ERA-Interim reanalysis: Configuration and performance of the data assimilation system. *Quart. J. Roy. Meteor. Soc.*, **137**, 553–597, https://doi.org/10.1002/qj.828.

Duan, A. M., J. Hu, and Z. X. Xiao, 2013: The Tibetan Plateau summer monsoon in the CMIP5 simulations. *J. Climate*, **26**, 7747–7766, https://doi.org/10.1175/JCLI-D-12-00685.1.

Fallah, B., U. Cubasch, K. Prömmel, and S. Sodoudi, 2016: A numerical model study on the behaviour of Asian summer monsoon and AMOC due to orographic forcing of Tibetan Plateau. *Climate Dyn.*, **47**, 1485–1495, https://doi.org/10.1007/s00382-015-2914-5.

Franklin, C. N., Z. A. Sun, D. H. Bi, M. Dix, H. L. Yan, and A. Bodas-Salcedo, 2013a: Evaluation of clouds in ACCESS using the satellite simulator package COSP: Global, seasonal, and regional cloud properties. *J. Geophys. Res.*, **118**, 732–748, https://doi.org/10.1029/2012JD018469.

Franklin, C. N., Z. A. Sun, D. H. Bi, M. Dix, H. L. Yan, and A. Bodas-Salcedo, 2013b: Evaluation of clouds in ACCESS using the satellite simulator package COSP: Regime-sorted tropical cloud properties. *J. Geophys. Res.*, **118**, 6663–6679, https://doi.org/10.1002/jgrd.50496.

Fu, Q., K. N. Liou, M. C. Cribb, T. P. Charlock, and A. Grossman, 1997: Multiple scattering parameterization in thermal infrared radiative transfer. *J. Atmos. Sci.*, **54**, 2799–2812, https://doi.org/10.1175/1520-0469(1997)054<2799:MSPITI>2.0.CO;2.

Fu, Y. F., and G. S. Liu, 2007: Possible misidentification of rain type by TRMM PR over Tibetan Plateau. *Journal of Applied Meteorology and Climatology*, **46**, 667–672, https://doi.org/10.1175/JAM2484.1.

Gao, Y. X., S. K. Jiang, and Y. G. Zhang, 1982: *Climatology of the Tibetan Plateau*. Science Press. Beijing, 300 pp. (in Chinese)

Hu, L., D. F. Deng, X. D. Xu, and P. Zhao, 2017: The regional differences of Tibetan convective systems in boreal summer. *J. Geophys. Res.*, **122**, 7289–7299, https://doi.org/10.1002/2017JD026681.

Huffman, G. J., R. F. Adler, D. T. Bolvin, and E. J. Nelkin, 2010: The TRMM multi-satellite precipitation analysis (TMPA). *Satellite Rainfall Applications for Surface Hydrology*, M. Gebremichael and F. Hossain, Eds., Springer, 3–22, https://doi.org/10.1007/978-90-481-2915-7_1.

IPCC, 2007: *Climate Change 2007*: *The Physical Science Basis*. Cambridge University Press, 446–727.

Jayakumar, A., J. Sethunadh, R. Rakhi, T. Arulalan, S. Mohandas, G. R. Iyengar, and E. N. Rajagopal, 2017: Behavior of predicted convective clouds and precipitation in the high-resolution Unified Model over the Indian summer monsoon region. *Earth and Space Science*, **4**, 303–313, https://doi.org/10.1002/2016EA000242.

Kummerow, C., and Coauthors, 2001: The evolution of the Goddard Profiling Algorithm (GPROF) for rainfall estimation from passive microwave sensors. *J. Appl. Meteor.*, **40**, 1801–1820, https://doi.org/10.1175/1520-0450(2001)040<1801:TEOTGP>2.0.CO;2.

Liu, Y., B. J. Hoskins, M. Blackburn, 2007: Impact of Tibetan orography and heating on the summer flow over Asia. *J. Meteor. Soc. Japan*, **85**, 1–19.

Luo, S., Z. A. Sun, X. G. Zheng, L. Rikus, and C. Franklin, 2016: Evaluation of ACCESS model cloud properties over the Southern Ocean area using multiple-satellite products. *Quart. J. Roy. Meteor. Soc.*, **142**, 160–171, https://doi.org/10.1002/qj.2641.

Luo, Y. L., R. H. Zhang, W. M. Qian, Z. Z. Luo, and X. Hu, 2011: Intercomparison of deep convection over the Tibetan Plateau-Asian monsoon region and subtropical North America in boreal summer using CloudSat/CALIPSO data. *J. Climate*, **24**, 2164–2177, https://doi.org/10.1175/2010JCLI4032.1.

Marchand, R., G. G. Mace, T. Ackerman, and G. Stephens, 2008: Hydrometeor detection using *Cloudsat* - An earth-orbiting 94-GHz cloud radar. *J. Atmos. Oceanic Technol.*, **25**, 519–533, https://doi.org/10.1175/2007JTECHA1006.1.

Maussion, F., D. Scherer, R. Finkelnburg, J. Richters, W. Yang, and T. Yao, 2011: WRF simulation of a precipitation event over the Tibetan Plateau, China — An assessment using remote sensing and ground observations. *Hydrology and Earth System Sciences*, **15**, 1795–1817, https://doi.org/10.5194/hess-15-1795-2011.

Pinker, R. T., and I. Laszlo, 1992: Modeling surface solar irradiance for satellite applications on a global scale. *J. Appl. Meteor.*, **31**, 194–211, https://doi.org/10.1175/1520-0450(1992)031<0194:MSSIFS>2.0.CO;2.

Pokharel, B., and G. Vali, 2011: Evaluation of collocated measurements of radar reflectivity and particle sizes in ice clouds. *Journal of Applied Meteorology and Climatology*, **50**, 2104–2119, https://doi.org/10.1175/JAMC-D-10-05010.1.

Stein, T. H. M., D. J. Parker, R. J. Hogan, C. E. Birch, C. E. Holloway, G. M. S. Lister, J. H. Marsham, and S. J. Woolnough, 2015: The representation of the West African monsoon vertical cloud structure in the Met Office Unified Model: An evaluation with CloudSat. *Quart. J. Roy. Meteor. Soc.*, **141**, 3312–3324, https://doi.org/10.1002/qj.2614.

Walters, D., and Coauthors, 2017: The met office unified model global atmosphere 6.0/6.1 and JULES global land 6.0/6.1 configurations. *Geoscientific Model Development*, **10**, 1487–1520, https://doi.org/10.5194/gmd-10-1487-2017.

Wang, C. H., H. X. Shi, H. L. Hu, Y. Wang, and B. K. Xi, 2015: Properties of cloud and precipitation over the Tibetan Plateau. *Adv. Atmos. Sci.*, **32**, 1504–1516, https://doi.org/10.1007/s00376-015-4254-0.

Webb, M., C., Senior, S. Bony, et al. 2001: Combining ERBE and ISCCP data to assess clouds in the Hadley Centre, ECMWF and LMD atmospheric climate models. *Climate Dyn*, **17**, 905–922, https://doi.org/10.1007/s003820100.

Winker, D. M., and Coauthors, 2010: The calipso mission: A global 3D view of aerosols and clouds. *Bull. Amer. Meteor. Soc.*, **91**, 1211–1230, https://doi.org/10.1175/2010BAMS3009.1.

Wu, G. X., and Y. S. Zhang, 1998: Tibetan Plateau forcing and the timing of the monsoon onset over south Asia and the South China Sea. *Mon. Wea. Rev.*, **126**, 913–927, https://doi.org/10.1175/1520-0493(1998)126<0913:TPFATT>2.0.CO;2.

Wu, G. X., and Coauthors, 2015: Tibetan Plateau climate dynamics: Recent research progress and outlook. *National Science Review*, **2**, 100–116, https://doi.org/10.1093/nsr/nwu045.

Xie, P. P., and P. A. Arkin, 1997: Global Precipitation: A 17-Year monthly analysis based on gauge observations, satel-

lite estimates, and numerical model outputs. *Bull. Amer. Meteor. Soc.*, **78**, 2539–2558, https://doi.org/10.1175/1520-0477(1997)078<2539:GPAYMA>2.0.CO;2.

Yan, Y. F., Y. M. Liu, and J. H. Lu, 2016: Cloud vertical structure, precipitation, and cloud radiative effects over Tibetan Plateau and its neighboring regions. *J. Geophys. Res.*, **121**, 5864–5877, https://doi.org/10.1002/2015JD024591.

Zhang, T. P., P. W. Stackhouse, S. K. Gupta, S. J. Cox, and J. C. Mikovitz, 2015: The validation of the GEWEX SRB surface longwave flux data products using BSRN measurements. *Journal of Quantitative Spectroscopy and Radiative Transfer*, **150**, 134–147, https://doi.org/10.1016/j.jqsrt.2014.07.013.